Journal of Applied Electrochemistry **33**: 703–708, 2003.

AISI 304 L stainless steel decontamination by a corrosion process using cerium IV regenerated by ozone
Part I: Study of the accelerated corrosion process

J.P. CAIRE[1], F. LAURENT[1], S. CULLIE[1], F. DALARD[1], J.M. FULCONIS[2] and H. DELAGRANGE[2]
[1]*LEPMI, ENSEEG, UMR 5631 INPG - CNRS, 1130 Rue de la Piscine, 38402 Saint-Martin d'Hères, France*
[2]*CEA Valrho, BP 171, 30207, Bagnols sur Cèze, France*
*(*author for correspondence, e-mail: Francis.Dalard@lepmi.inpg.fr)*

Received 8 January 2001; accepted in revised form 21 March 2003

Key words: cerium, corrosion, decontamination, ozone, stainless steel

Abstract

This paper describes the study of a new decontamination process of AISI 304L stainless steel from dismantled nuclear power plants. A very thin active contaminated surface layer was stripped from the underlying metal by corrosion in a solution of nitric acid with the addition of cerium nitrate. The Ce^{4+}/Ce^{3+} concentration ratio was initially equal to unity and ozone/oxygen bubbles were used to regenerate Ce^{3+} ions into Ce^{4+} ions. The study was performed in a laboratory cell prior to preliminary optimization in a three-litre reactor. The objective was to obtain a corrosion rate of about 10 micrometers per day. This target was reached in 10^{-2} mol l^{-1} of cerium nitrate with bubbling of a 1.56 g h^{-1} ozone flow in a 60 l h^{-1} total gas flow. The corrosion rate depended essentially on the Ce^{4+} concentration. The stainless steel exhibited intergranular corrosion. The corrosion rate was monitored by measuring the solution oxidizing potential using a precious metal electrode.

1. Introduction

Arvesen [1, 2] studied different alternatives for decommissioning the components of PWR nuclear power plants. When an irradiated nuclear plant is dismantled, the large, irregular-shaped waste surfaces must undergo a thorough preliminary decontamination process in order (i) to reduce as much as possible the radioactivity of the largest part of the wastes and minimize the amount of secondary diluted wastes, and (ii) to make the dismantling process easier by reducing the difficult and costly mechanical operations by remote manipulators. To fulfil these goals, the preliminary decontamination must be done *in situ*. The process involves extracting the radioactive elements found mainly at the surface. This can be done by corrosion. Acid attack of the first 10-micrometer layer of the wall metal substrate can be performed to make the process easier.

Different processes have been suggested to achieve the above requirements. Trials have been conducted on the use of an electropolishing process [3], electric breakdown of the oxide layer [4] and chemical corrosion of the surface [5]. Suwa et al. [6] proposed a decontamination process using a sulfuric acid–cerium solution for reactor dismantling in 1988. Klein et al. [7–10] developed a chemical process using cerium for the decontamination of a dismantled PWR primary loop in Belgium. In France, Dubourg [11] published results obtained by use of a similar chemical process designed for decontamination of 600-nickel alloy tubes from the vapour generators of the Tricastin nuclear plant. The process decreased the tube activity from 70000 to 14 Bq cm^{-2}.

Due to the complexity of the present study, it was divided into two main parts:

(a) a process feasibility study involving experiments in a beaker and a three-litre micro pilot,
(b) a modelling and optimization study of the process using the same micro pilot.

In this paper we describe a study of the corrosion rate of AISI 304 L stainless steel in a nitric acid medium, the ultimate goal being to optimize the process. In such a medium, even in the presence of ozone and oxygen bubbles, the corrosion rate of stainless steel is low. The presence of cerium IV ions is known to accelerate corrosion [1]. To design the process, it was first necessary to study the physicochemical operating conditions needed to achieve the goal. A comparative study revealed the relative effects of the different parameters involved in the study, namely: nitric acid, total cerium concentrations, flow and temperature of the oxidizing solution. The main industrial goals were: (i) a target corrosion rate of 10 micrometers per day, and (ii) corrosion restricted to the sample surface.

2. Constraints

After decontamination, radioactive liquid wastes are eliminated by vitrification. This type of process requires low cerium concentrations in the waste material so as to avoid dangerous weakening of the cast glass. It is also important to avoid pitting corrosion, which results in the dissolution of some sound metal parts. The corrosion rate must be kept low to ensure uniform attack limited to a very thin radioactive layer. The most convenient duration of the process is one day, which would require a corrosion rate of 10 μm per day. All these constraints were taken into account.

3. The process

The aim of the process is to dissolve a very thin contaminated layer through the use of cerium in a nitric acid solution. Cerium is a strong oxidizer [1]. The corrosion reaction is

$$n\mathrm{Ce}^{4+} + \mathrm{M} \rightarrow n\mathrm{Ce}^{3+} + \mathrm{M}^{n+} \quad (1)$$

where M represents one of the constitutive metals in the alloy of interest, namely, Fe, Cr and Ni. Table 1 presents the composition of AISI 304L stainless steel. The total cerium concentration was varied for each experiment, but the initial Ce^{4+}/Ce^{3+} concentration ratio was maintained at unity. Since corrosion ceases with the disappearance of Ce^{4+} ions, a regeneration process had to be found. Ozone was chosen to produce the following reaction:

$$2\,\mathrm{Ce}^{3+} + \mathrm{O_3} + 2\,\mathrm{H}^{+} \rightarrow 2\,\mathrm{Ce}^{4+} + \mathrm{H_2O} + \mathrm{O_2} \quad (2)$$

It was assumed that the ozone concentration remained sufficiently low to have no influence on the corrosion rate of the stainless steel.

4. Experimental details

4.1. *Electrochemical cell*

The electrochemical study was conducted at 25 °C in the Metrohm electrochemical cell shown in Figure 1. Three electrodes were connected to a potentiostat–galvanostat (Radiometer Voltalab, Villeurbanne, France) driven by an electronic interface associated with Voltamaster software: (i) a rotating working electrode (Radiometer EDI 101 T) equipped with a 0.031 cm^2 disc made of either platinum or AISI 304 L stainless steel; (ii) a saturated calomel reference electrode (E_{SCE}) placed in an extension containing a saturated potassium nitrate solution (Radiometer X100); and (iii) a 1 cm^2 auxiliary electrode in platinum.

Table 1. Composition of AISI 304 L stainless steel

Elements	Fe	Ni	Cr	C	Si	Mn	S	P
Weight %	69.17	10.0	18.0	<0.03	0.75	<2	0.015	0.04

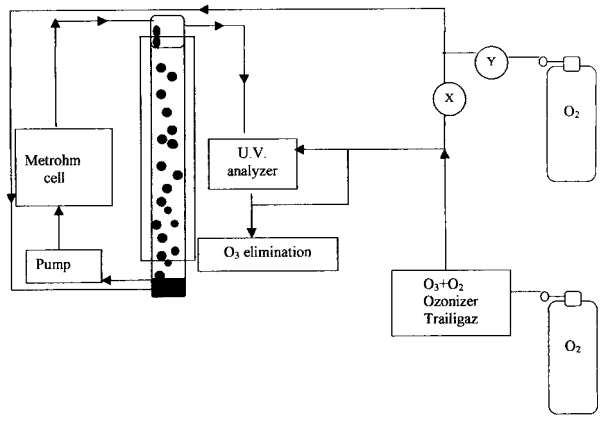

Fig. 1. Metrohm electrochemical cell and pilot reactor (X,Y mass flow controllers).

The electrolyte was a 4 mol l^{-1} nitric acid solution with the addition of cerium nitrate and an initial Ce^{3+}/Ce^{4+} concentration ratio of unity. Ozone was introduced into the solution by means of oxygen–ozone bubbling. The mass flow of the oxygen–ozone mixture was kept at a constant rate of 60 g h^{-1} with the possibility of varying the O_2/O_3 mass flow ratio.

The experimental apparatus was able to record the rest potential and plot the polarization curves. The 10 mV s^{-1} potential sweep rate was sufficiently low for a pseudo steady state to be assumed. The working electrode was an AISI 304 L stainless steel disc to record the corrosion current. The same experiments were performed using platinum electrodes to measure the potential of the oxidizing solution in the cell.

4.2. *Pilot reactor*

The three-litre pilot reactor (Figure 1) was used to approximate the experimental conditions of an industrial reactor. This reactor was made of a glass column functioning as a counter-current bubble column. The column had a glass jacket allowing easy control of its internal temperature. The ozonizer was fed with pure oxygen to avoid any interference with nitrogen compounds. The ozone–oxygen mixture was injected into the reactor by means of a porous sieve distributor placed at the column bottom. A 150 l h^{-1} pump recycled the oxidizing solution flow from bottom to top of the column. The ozone mass transfer was due to the small ascending bubbles generated through the sieve. The ozone concentration was measured at both reactor inlet and outlet by a Trailigaz U.V. spectrophotometer. The AISI 304 L stainless steel test specimen placed in the test reactor was cylindrical in shape (4.5 cm inner diameter, 4.8 cm outer diameter, 10.5 cm height). The following electrodes were put at carefully chosen places inside the

reactor for monitoring the corrosion process: (i) a saturated calomel reference electrode (SCE) in an extension containing a KNO_3 saturated solution; (ii) a rod made of AISI 304L stainless steel placed on the steel cylindrical specimen and acting as an electrode to measure the corrosion potential of the specimen (V vs SCE). The specimen was washed successively in acetone and ethyl alcohol and rinsed with distilled water; and (iii) a wire platinum electrode to monitor the potential of the oxidizing solution in the reactor (V vs SCE). All three electrodes (reference, stainless steel and platinum) were linked to a Keithley multimeter driven by an electronic interface and Test Point software.

The conditions in the reactor were as follows: (a) the total cerium nitrate concentration varied from 5×10^{-3} mol l^{-1} to 5×10^{-2} mol l^{-1}. The Ce^{4+}/Ce^{3+} concentration ratio was equal to one at the beginning of each experiment; (b) the ozone concentration was kept constant. The mass flow of ozone was maintained at 6 g h^{-1} in a total gas flow of 60 l h^{-1}; and (c) the nitric acid concentration was set at 4 mol l^{-1}. In these working conditions, the potential of the solution and the corrosion potential of the AISI 304L stainless steel cylinder were measured on-line. The corrosion rate was obtained at constant time intervals by means of gravimetric weight-loss measurements. The standard protocol gave a 0.02 g precision. Total interruptions for measurement amounted to less than half an hour. We verified that the interruptions did not modify either the volume or composition of the solution in such conditions. Other characteristics of the solution and metal were obtained by analysis after complete removal of the solution.

4.3. *Analysis of oxidizing solutions*

Solution samples removed periodically from the reactor were analysed with a Perkin–Elmer ICP. Since total removals represented less than 3% of the initial volume of solution, it was assumed that they did not modify the operating conditions of the reactor. The solutions were analysed by cathodic sweep voltammetry on a Au or Pt rotating disc in the Metrohm electrochemical cell described above.

5. Experimental results

5.1. *Preliminary study in beaker*

The study in the beaker was conducted to evaluate the influent parameters leading to the corrosion of the AISI 304 L stainless steel specimen. The standard oxidation-reduction potentials of the species present in the electrolyte are given in Table 2. On the basis of these values, it was assumed that the possible mainsprings of AISI 304L corrosion were the O_3, O_2, NO_3^- and Ce^{4+} elements.

The individual role played by these elements in the process was evaluated by means of polarization curves.

Table 2. Standard oxidation-reduction potentials

Redox couple	Standard potential vs NHE /V
O_3/O_2	2.07
Ce^{4+}/Ce^{3+}	1.72
HNO_3/HNO_2	0.94

Table 3. Corrosion current density of AISI 304 L stainless steel in 4 mol l^{-1} HNO_3 with or without ozone flow and with or without 0.25 mol l^{-1} cerium nitrate

Solution	HNO_3	$HNO_3 + O_3$	$HNO_3 + O_3 + Ce^{4+}$
i_{corr}/A cm^{-2}	6.4×10^{-11}	1.0×10^{-10}	6.3×10^{-5}

The curves were plotted by means of the rotating AISI 304 electrode in 4 mol l^{-1} nitric acid solutions containing cerium nitrate in the presence of oxygen–ozone bubbles. The electrolyte was assumed to be saturated in oxygen and ozone. The respective saturation concentrations of oxygen and ozone were as low as 10 ppm and 1.5 ppm in these conditions [12].

The corrosion current density i_{corr} was obtained by measuring the limiting current density. Given the corrosion current density of AISI 304 L in Table 3, Ce^{4+} appeared to be the most likely corrosion mainspring. Measurements of i_{corr} showed that the presence of Ce^{4+} in the solution accelerated corrosion of the stainless steel in the experimental conditions. Cerium IV efficiency was probably due to its good solubility (the solubility of ozone and oxygen is comparatively low in the medium).

An increase in the cerium concentration in the solution led to a visible rise in the corrosion current density (Figure 2). The evolution of the corrosion potential observed in Figure 3 can be attributed to an increase in the Ce^{4+}/Ce^{3+} ratio due to the presence of ozone bubbles.

5.2. *Stainless steel corrosion in the pilot reactor*

The corrosion conditions in any reactor can be very different locally from those in a beaker. Such differences are understandable given such factors as the circulation of gas and liquid, the volumes of liquid involved, the shape and the dimensions of corroded surfaces and stirring. The experiments lasted 12 h. In such conditions, we observed the presence of small metallic grains retained by the sieve. These small grains were assumed to come from intergranular corrosion. Thus, corrosion of the steel generated Cr^{6+} and Fe^{3+} ions that could play a significant role in the corrosion process by afterwards constituting new corrosive agents.

With a view to process optimization, the different parameters of interest were studied. In the next paragraphs, we describe the respective influence of each parameter on the corrosion process determined on the

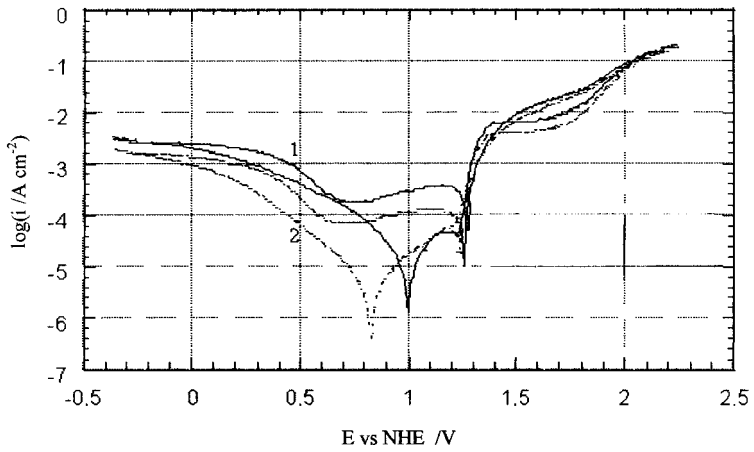

Fig. 2. Polarization curves of AISI 304 L stainless steel against Ce concentration in 4 mol l^{-1} nitric acid solution with O_2 and O_3 bubbles at 298 K. (1) [Ce] = 1×10^{-2} mol l^{-1}; (2) [Ce] = 1×10^{-3} mol l^{-1}.

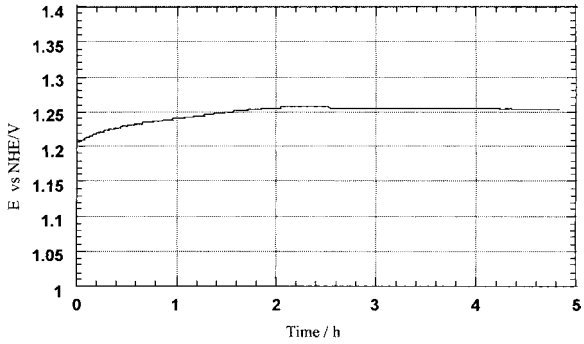

Fig. 3. Corrosion potential of AISI 304 L stainless steel against time in 4 mol l^{-1} HNO_3 and 1×10^{-2} mol l^{-1} $CeNO_3$ solution with O_2 and O_3 bubbles at 298 K.

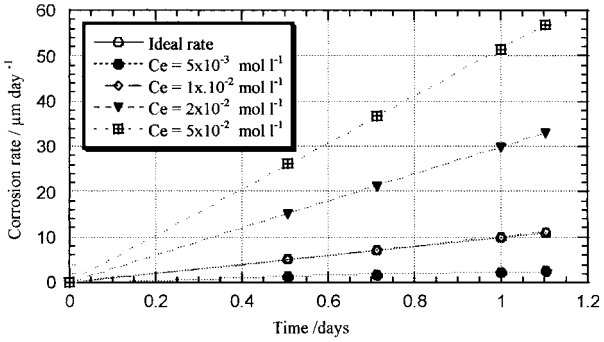

Fig. 4. Gravimetric corrosion rates against Ce concentration in a 4 mol l^{-1} nitric acid solution with O_2 and O_3 bubbles at 298 K.

basis of modifications appearing on the specimen after corrosion.

5.2.1. *Role of ozone*

To demonstrate the effect of ozone, tests were performed for 12 h in the following conditions: (i) 6 g h^{-1} ozone mass flow rate; (ii) 60 l h^{-1} oxygen-ozone flow rate in the column; and (iii) 30 l h^{-1} solution circulating flow rate.

During the preliminary tests performed without cerium ions in the solution, no variation in the mass of the specimen was observed. This observation confirmed that the ozone–oxygen–nitric acid mixture alone did not directly corrode the stainless steel.

When the ozone flow was stopped, the potential decreased by 200 mV in less than half an hour. It was concluded that the steel corrosion rate dropped rapidly when the Ce^{4+} ions were not regenerated, indicating the need for Ce^{4+} regeneration by ozone.

5.2.2. *Role of cerium*

The stainless steel corrosion rate for different total cerium concentrations in solution was determined by gravimetry. For each run, the oxygen–ozone flow was bubbled with a 1/1 initial Ce^{4+}/Ce^{3+} ratio in the nitric acid solution, as previously. It should be noted that no weight loss was observed when the specimen was immersed in the electrolyte without cerium. The corrosion rate (Figure 4) confirmed that the cerium Ce^{4+} concentration played a key role in the corrosion process. This result is in good agreement with the results obtained in the laboratory cell.

5.2.3. *Role of Cr^{6+} and Fe^{3+} ions*

The corrosion potential of the steel in the reactor became stabilized at $E_{corr} = 1.25$ V vs NHE (Figure 3). Given this potential value on the cathodic polarization curve in Figure 2, it was concluded that the equilibrium potentials of the two oxidation–reduction couples Fe^{3+}/Fe^{+2} and Cr^{6+}/Cr^{3+} were lower than the corrosion potential of the sample and that these ions were not the mainsprings of steel corrosion at this corrosion potential.

5.3. *Morphology of corrosion*

5.3.1. *SEM observations*

The grain boundaries appeared sharply on the micrographs of the sample surface before corrosion. This was probably due to the successive processes involved in making the tube. The micrograph of a transverse cross section after corrosion (Figure 5) shows an intergranular attack of the 304 L stainless steel limited to less than

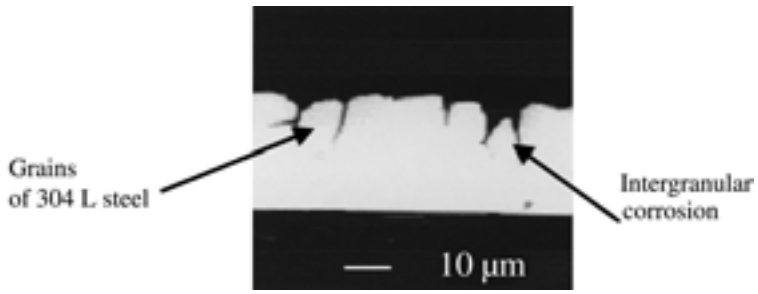

Fig. 5. Cross section of a 304 L stainless steel tube after corrosion in a 4 mol l^{-1} nitric acid solution with O_2 and O_3 bubbles at 298 K.

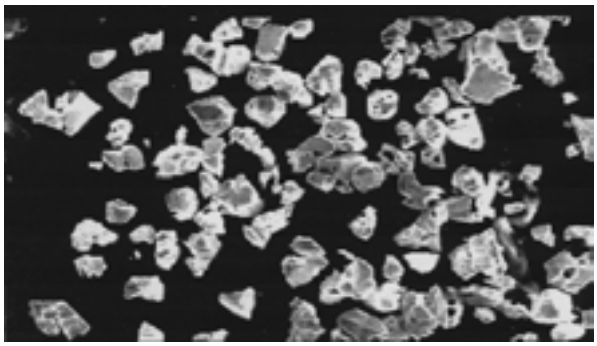

Fig. 6. AISI 304 L stainless steel grains resulting from corrosion and found in the reactor dead zones in a 4 mol l^{-1} nitric acid solution with O_2 and O_3 bubbles at 298 K. Magnification × 500.

ten micrometers of thickness and an absence of pitting. This type of corrosion has already been reported in similar conditions [13]. No evidence of irregularity appeared beyond ten micrometers of thickness, so that the initial requirement of uniform corrosion was met.

It should be noted that intergranular corrosion caused the detachment of some grains from the 304 L stainless steel. Such grains were found in the dead zones of the reactor after the corrosion process. Figures 5 and 6 show that the grain size was uniform and close to 10 μm. The question of what happened to these grains in the reactor must be considered. After their detachment from the surface, the grains continued to corrode. This factor must therefore be taken into account in the mass balances. The kinetics of grain detachment from the sample surface can be assessed by calculating the difference between the weight loss of the sample and the quantity of Fe^{3+}, Ni^{2+}, Cr^{6+} ions found in the solution after the corrosion process. The results of ICP analyses of the solutions after corrosion (Figure 7) showed that, after 24 h of corrosion, the detached grains found in the dead zones of the reactor represented approximately 10% of the weight loss of the sample.

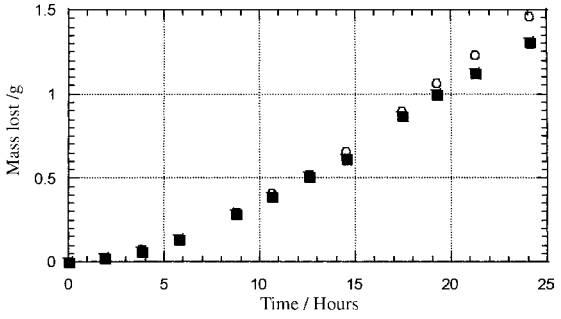

Fig. 7. Comparison of corrosion product masses and mass in solution against time. Key: (○) mass lost; (■) mass measured by ICP.

5.3.2. *Changes in the active surface during the corrosion process*

The active surface of the steel specimen increased with time due to intergranular attack and the subsequent detachment of grains. Since the corrosion rate of the specimen was related to its active surface, the corrosion rate must have increased during the corrosion process. Given that the detached grains in the dead zones of the reactor could represent 10% of the weight loss after 24 h, estimation of the corrosion rate was difficult. Both corrosion rates calculated from measurements (direct analysis of ions in solution or limiting currents) were obviously underestimated.

5.4. *Study of corrosion rate*

The CeO_2 content of vitrified glass has to be very low, otherwise the glass will be dangerously weakened. The wastes from the decontamination process must therefore be very low in cerium.

Another constraint concerns the risks of deep intergranular corrosion, which could transfer sound metal into the solution. To avoid this unwanted phenomenon, the corrosion rate must be kept to a relatively low level. The initial target of 10 μm per day was chosen as a good compromise compatible with the previous requirements.

The steel corrosion rate is related essentially to the cerium concentration and the quantity of ozone used for Ce^{4+} regeneration. The optimum cerium concentration therefore had to be determined to obtain a compromise between corrosion rate, corrosion uniformity and the cost of reprocessing secondary wastes. Figure 4 shows that the 10 μm per day goal for the corrosion rate was obtained at 25 °C for a cerium concentration of 1×10^{-2} mol l^{-1}. In such conditions, the corrosion effect appeared to be limited to the thin contaminated layer.

5.5. *Sensor and process control*

The process required a sensor that would be reliable and stable in the aggressive medium and which could monitor the corrosion progress in the reactor on-line.

These requirements for reactor control could be met by electrochemical measurement of the oxidizing potential of the solution using a platinum electrode. This type of sensor has many advantages, namely simplicity, good corrosion resistance and low cost on-line monitoring. This would be an efficient solution if the potential of a precious metal electrode (platinum or gold) was a function simply of the Ce^{4+} content in the solution. In fact, it should be emphasised that the presence of the other ions and bubbling of the oxygen–ozone mixture led to a mixed potential which was difficult to interpret. Fortunately, the experiments showed that this mixed potential was particularly sensitive to the Ce^{4+}/Ce^{3+} concentration ratio in the nitric acid solution. Thus, it is possible to assimilate the mixed potential of a platinum (or gold) electrode to the equilibrium potential of the Ce^{4+}/Ce^{3+} oxidation–reduction couple.

Using the previous assumptions, when the regeneration process is active, concentrations and solution potential are those of a nernstian electrode. Figure 8 presents the changes in potential with time of the platinum electrode vs NHE. The potential changed because of the sensitivity of this electrode to the Ce^{4+}/Ce^{3+} concentration ratio. Therefore, the increase in the oxidizing potential of the solution since the beginning of experiment when bubbling started can obviously be attributed to the immediate oxidation of cerium Ce^{3+} by ozone.

In this respect, the corrosion current density of the AISI 304 L stainless steel was proportional to the Ce^{4+} concentration. The variation in the corrosion current density infers a similar variation in the corrosion rate. On-line control of the reactor could thus be achieved by a simple system of a platinum electrode providing information on the solution potential, with this information being used to adjust the ozone mass flow in the reactor.

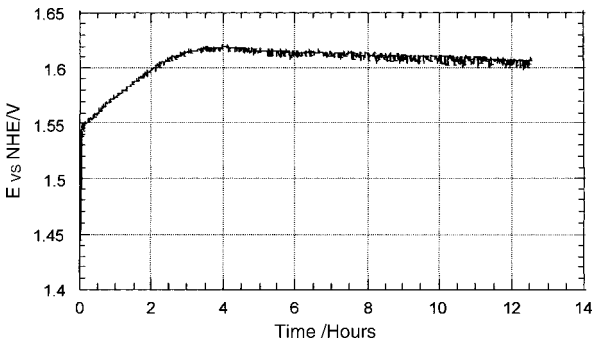

Fig. 8. Changes in potential of an oxidizing solution containing 4 mol l^{-1} nitric acid and 1×10^{-2} mol l^{-1} cerium concentrations against time.

6. Conclusions

The Ce^{4+} ions were the main agent of the corrosion process for AISI 304 L. In the presence of a bubbled oxygen–ozone mixture in nitric acid electrolyte, the total concentration of Ce^{3+} and Ce^{4+} ions was effectively related to the corrosion rate of the AISI 304 L alloy. Although the ozone was not responsible for the corrosion process, it controlled the regeneration of Ce^{4+} required for corrosion to take place.

The initial target of a 10 μm per day corrosion rate was achieved with a 10^{-2} mol l^{-1} cerium concentration, a 1.56 g h^{-1} ozone mass flow and a 60 l h^{-1} total gas flow. In these conditions, the micrographs exhibited an acceptable surface appearance**.** Inter-granular corrosion appeared to be limited to the first grain layer. Grain detachment was observed in the reactor and its contribution was estimated at 10% of the weight loss.

It was established that corrosion could be monitored by simple measurement of the oxidizing potential of the solution. Such monitoring can be performed by reliable, low-cost potential measurement using a platinum or gold electrode.

The Ce^{4+}, Cr^{6+} and Fe^{3+} concentrations could be determined from the limiting currents obtained from cathodic voltammetry. Monitoring of the changes in these concentrations over time could offer another valuable method of process control.

References

1. J. Arvesen, Studsvick Energiteknik AB, *SE Patent WO 85/04279* (9 March 1984).
2. J. Arvesen, Studsvick Energiteknik AB, *SE Patent WO 90/01774* (11 Aug. 1988).
3. J.N. Saas, J.P. Gauchon and F. Dalard, *J. Chem. Phys*. **95** (1998) 1.
4. L. Abiven, F. Dalard, J.J. Rameau, C. Cauchaud and P. Funtes, *Revue de Métallurgie*, SGM, Feb. (1998) 1.
5. M. Dubourg, *Nucl. Eng. Des*. **159** (1995) 123.
6. T.T. Suwa, N. Kuribayashi and E. Tachikawa, *Corros. Eng*. **37** (1988) 73.
7. M. Klein, M. Ponnet and A. Rahier, *BE Patent WO 99/43006* (22 Feb. 1999).
8. M. Ponnet, M. Klein, A. Rahier, L. Noynaert and L. Aleton, 8th International Conference on 'Radioactive Waste Management and Environmental Remediation', Bruges, Belgium, 30 Sept.–4 Oct. (2001).
9. J. Dadoumont, V. Massaut, M. Klein and Y. Demeulemeester, 8th International Conference on 'Nuclear Engineering', Baltimore, 2–6 Apr. (2000).
10. M. Klein and S. Moers, ICRM Conference on 'Low Level Radioactivity Measurement Techniques', Mol, Belgium, 18–22 Oct. (1999).
11. M. Dubourg, *French Patent 93 01107* (2 Feb. 1993).
12. P. Pascal, 'Nouveau traité de Chimie Minérale', Tome 13, (Masson, Paris 1960), p. 254.
13. P. Lacombe, B. Baroux and G. Beranger, '*Les aciers inoxydables*' (Les Editions de Physique, Paris, 1990), p. 414.
14. J.A. Wharton, B.G. Mellor, R.J.K. Wood and C.J.E. Smith, *J. Electrochem. Soc*. **147** (2000) 3294.